Non-linear magnetohydrodynamic simulations of Edge Localised Modes triggering via vertical oscillations

F.J. Artola[1,5], G.T.A. Huijsmans[2,3], M. Hoelzl[4], P. Beyer[1], A. Loarte[5], and Y. Gribov[5]

[1] *Aix-Marseille Université, CNRS, PIIM UMR 7345, 13397 Marseille, France*
[2] *CEA, IRFM, F-13108 St. Paul-lez-Durance cedex, France*
[3] *Eindhoven University of Technology, Eindhoven, The Netherlands*
[4] *Max Planck Institute for Plasmaphysics, Boltzmannstr. 2, 85748 Garching, Germany*
[5] *ITER Organization, Route de Vinon sur Verdon, 13067 St Paul Lez Durance Cedex, France*

Email: javier.artola-such@univ-amu.fr

Abstract

Magnetic triggering of Edge Localized Modes (ELMs) in ohmic H-mode plasmas was first reported in the TCV tokamak [1]. This method, showing reliable locking of the ELM frequency to an imposed axisymmetric vertical plasma oscillation, was also demonstrated in the ITER-relevant type-I ELM regime in ASDEX Upgrade [2] and JET [3]. However, the mechanisms of the ELM triggering due to a vertical motion has not been studied extensively. The non-linear reduced MHD code JOREK-STARWALL has been extended for 3D free-boundary computations [4], which has allowed us to simulate for the first time realistic vertical oscillations together with ELM simulations in a single consistent scheme. Our simulations demonstrate that stable plasmas can be destabilized by the application of a vertical oscillation. During the vertical motion, a toroidal current is induced in the pedestal. The origin of this current is analysed in detail with the use of simulations and a simple analytical model, revealing that it arises from the compression of the plasma cross section due to its motion through an inhomogeneous magnetic field. Initially lower pedestal currents require bigger vertical displacements to destabilize ELMs, which directly points towards the increased edge current as the ELM driving mechanism. Finally the ELM triggering shows a very weak dependence on the plasma velocity in agreement with experiments.

1 Introduction

Magnetic triggering of Edge Localized Modes (ELMs) in ohmic H-mode plasmas was first reported in the TCV tokamak [1]. The experiments showed that imposing a vertical plasma oscillation using poloidal field coils (PF coils), leads to a reliable locking of the ELM frequency to the vertical oscillation frequency. These vertical oscillations often called "vertical kicks" or "vertical jogs" were also used for ELM frequency control in the ITER-relevant type-I ELM regime in ASDEX Upgrade [2] and JET [3] tokamaks. This technique could play a crucial role in controlling the impurity content of the plasma and the energy released per ELM. For ITER, vertical oscillations are considered as a back-up technique [5] for the initial non-active operation at half current and half magnetic field (7.5MA, 2.65).

Linear stability studies were performed for vertical kick simulations for JET [3] and ITER [6]. These studies concluded that the main destabilizing factor was an increase of edge current produced by the oscillations, which is known to destabilize peeling-ballooning modes [7] . However the authors of [8] argued that for the AUG case, ELMs were destabilized when the edge current was decreasing and therefore, ELMs could be triggered by other more subtle factors such as the change in plasma shape or in pressure gradient. The main goal of this work is to clarify which is the determining factor for the ELM destabilization through non-linear simulations and as well, to provide an understanding of the current induction during the plasma motion. Our research is performed by using the code couple JOREK-STARWALL [4, 9, 10] as it allows 3D MHD non-linear simulations with free-boundary conditions. As well, a 3D thin resistive wall is available in JOREK-STARWALL and we have recently

included realistic PF coils that take into account all the mutual inductances of the system. All these features allow us to simulate for the first time realistic vertical oscillations together with ELM simulations in a consistent single scheme.

The paper is organized as follows, in section 2 we investigate the physics of the edge current induction during the plasma vertical motion, where we show analytical results and then we present simulations of both a simplified plasma and a realistic ITER scenario. In section 3 we analyse the non-linear stability of an ITER scenario during a vertical oscillation and we investigate the main causes of ELM destabilization. Finally we present our conclusions in section 4.

2 Understanding the axisymmetric induction of edge currents during vertical oscillations

The authors of [3] and [6] concluded that the mechanism underlying the ELM triggering was an increase of the edge toroidal current driving the plasma into the unstable MHD peeling-ballooning regime. The induction of edge toroidal current was mainly attributed to a fast reduction of the plasma volume due to the vertical motion through an inhomogeneous magnetic field. Here we investigate this effect analytically in the frame of an MHD model and we show simulations of both a simple elongated plasma and a realistic ITER 7.5MA/2.65T scenario.

In the following we aim to give some analytical insights into the current induction in a moving plasma. This effect can be understood by analysing the MHD equation for the poloidal flux ψ[1]

$$\frac{\partial \psi}{\partial t} + \mathbf{v} \cdot \boldsymbol{\nabla} \psi = \eta J_\phi \tag{1}$$

where t, $\mathbf{v}$, η, J_ϕ are respectively time, velocity, resistivity and toroidal current density. By separating the poloidal flux into a contribution of the plasma plus an external contribution ($\psi = \psi_p + \psi_{ext}$) and using the convective time derivative ($d/dt \equiv \partial_t + \mathbf{v} \cdot \boldsymbol{\nabla}$) (1) becomes

$$\frac{d\psi_p}{dt} = -\frac{\partial \psi_{ext}}{\partial t} - \mathbf{v} \cdot \boldsymbol{\nabla} \psi_{ext} + \eta J_\phi \tag{2}$$

In the reference frame of the plasma (i.e. following a flux surface) we find that

$$\delta\psi_p \approx -\delta\psi_{ext} + \eta J_\phi \delta t \tag{3}$$

where $\delta\psi_{ext} \approx \delta\psi_{ext}(\mathbf{r}_0) + \delta\mathbf{r} \cdot \boldsymbol{\nabla}\psi_{ext}$ and $\delta\mathbf{r}$ is the displacement of the flux surface. For an axisymmetric case, the plasma contribution to the poloidal flux can be written in terms of the plasma current

$$\psi_p(R,Z) = \mu_0 \int J_\phi(R',Z') G(R,Z,R',Z') dR' dZ' \tag{4}$$

where $G(R,Z,R',Z')$ is a Green's function given by [11]. The latter integral can be analytically calculated for a cylindrical plasma with a spatially constant current density $J_\phi(t)$ going from the radius r_0 to the plasma edge, which is given by $a(t) \equiv r_0 + w_r(t)$ (see Figure 1 a). With these assumptions the plasma poloidal flux is

$$\psi_p(a,t) \approx \psi_p(r_0) - B_\theta(r_0) R_0 w_r(t) - \frac{\mu_0}{4\pi} R_0 I_\phi^{w_r}(t) \tag{5}$$

where $I_\phi^{w_r}(t) = 2\pi r_0 w_r(t) J_\phi(t)$ is the total toroidal current contained in the edge region $r \in [r_0, a(t)]$ and we have also assumed that $w_r/r_0 \ll 1$. If we assume now that during the plasma motion the internal plasma moves rigidly without any change in the region $r \leq r_0$, equation (3) becomes

$$\delta I_\phi^{w_r} = \frac{4\pi}{\mu_0 R_0} \left[\delta\psi_{ext}(a) - B_\theta(r_0) R_0 \delta w_r - \eta J_\phi \delta t\right] \tag{6}$$

[1] here $\psi \equiv R_0 A_\phi$ where R_0 is the major radius and A_ϕ is the toroidal component of the magnetic vector potential

where $\delta\psi_{ext}(a) = \delta\psi_{ext}(a_0) + \delta\mathbf{r}\cdot\boldsymbol{\nabla}\psi_{ext}$ and the change of current density is

$$\delta J_\phi = \frac{1}{2\pi r_0 w_r}\left(\delta I_\phi^{w_r} - I_\phi^{w_r}\frac{\delta w_r}{w_r}\right) \tag{7}$$

From equations (6) and (7) we can extract the following conclusions:

- The total induced current $\delta I_\phi^{w_r}$ only depends on the speed of the motion (δt) through the resistive decay term, which can be considered to be small. Therefore there is no velocity dependence for an a ideal conductor.
- The total induced current $\delta I_\phi^{w_r}$ is induced by 3 mechanisms
  1. Due to a local change in external flux $\delta\psi_{ext}(a_0)$ (i.e. produced by time variation of currents in PF coils or walls).
  2. Due to the motion of the plasma through an inhomogeneous static magnetic field $\delta\mathbf{r}\cdot\boldsymbol{\nabla}\psi_{ext}$. For this effect, a gradient of external flux is required and plasma deformation also plays an important role through $\delta\mathbf{r}$.
  3. Due to plasma compression or expansion (δw_r).
- The variation of current density δJ_ϕ is inversely proportional to the radial width (w_r). This width could be approximated as the skin depth $w_r \sim \sqrt{\eta/(\pi\mu_0 f)}$, where f is the oscillation frequency.
- δJ_ϕ can be produced by two effects
  1. An increase in total current in the region of induction ($\delta I_\phi^{w_r}$).
  2. A change in the width of the region of induction δw_r (redistribution of current).

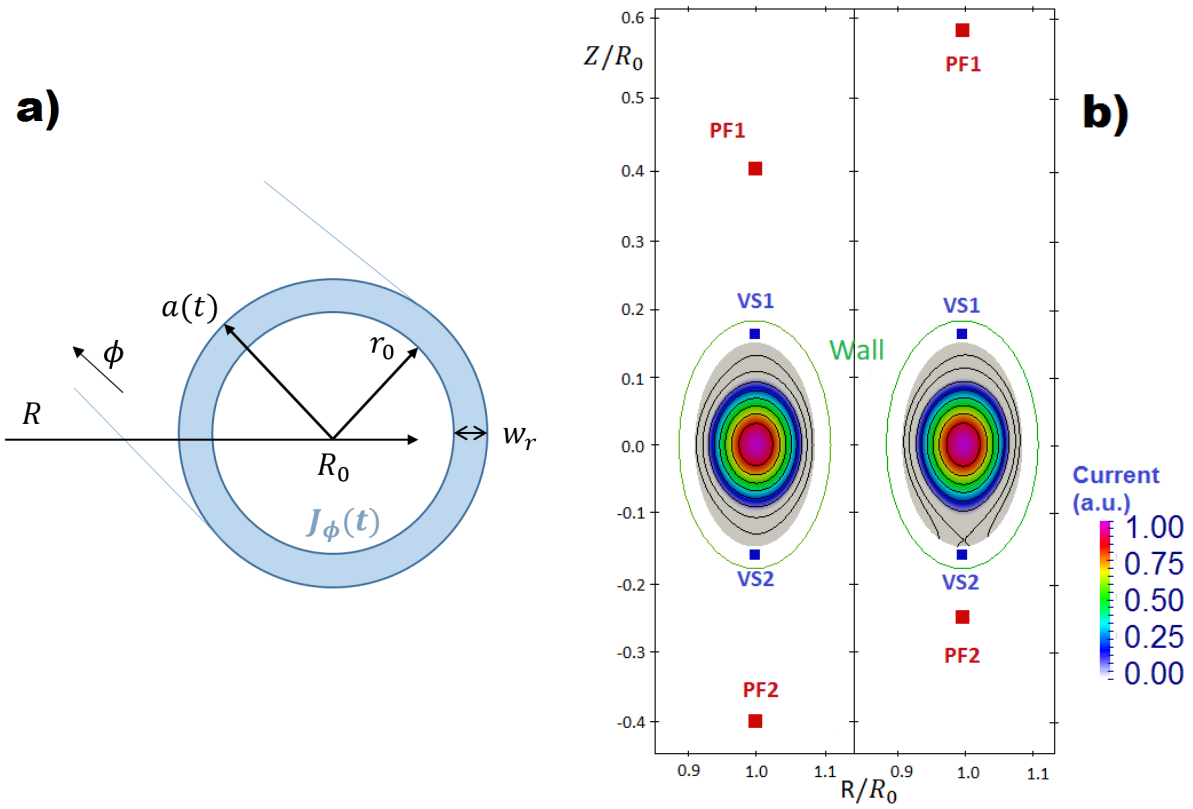

FIGURE 1: (a) Graphic representation of the cylindrical model used for the current induction analytical calculation. (b) The two different equilibrium configurations for the simple plasma case simulations.

2.1 Simple elongated plasma

In the following, we present the case of a simple elongated pressure-less plasma ($\beta_p \ll 1$) that vertically oscillates for 2 different PF coil configurations. For both cases (Figure 1 b) the inverse aspect ratio ($\epsilon = 0.07$), the elongation ($\kappa = 1.4$), the ratio between wall and plasma radius ($b_w/a = 1.6$), the plasma size, position and total toroidal current are the same. Besides the 2 PF coils (PF1,PF2) that elongate the plasma, we have also included 2 coils (VS1,VS2)[2] in which currents oscillate in a sinusoidal form. The latter are used to vary the plasma position over time. These simulations were performed with JOREK-STARWALL using the reduced MHD model presented on [9]. The used grid has a polar structure formed by 2200 bicubic Bezier elements, the maximum Lundquist number is $\sim 10^7$ and the magnetic Prandtl number is $\sim 10^{-5}$. We use a temperature dependent resistivity ($\eta \propto T^{-3/2}$) for these simulations, where the ratio between the vertical oscillation period and the plasma resistive time varies from 10^{-3} at the plasma core up to 10 at the plasma edge. As well, the ratio between plasma core and wall resistivity is 0.1. The perpendicular particle diffusivity and thermal conductivity are neglected for this study.

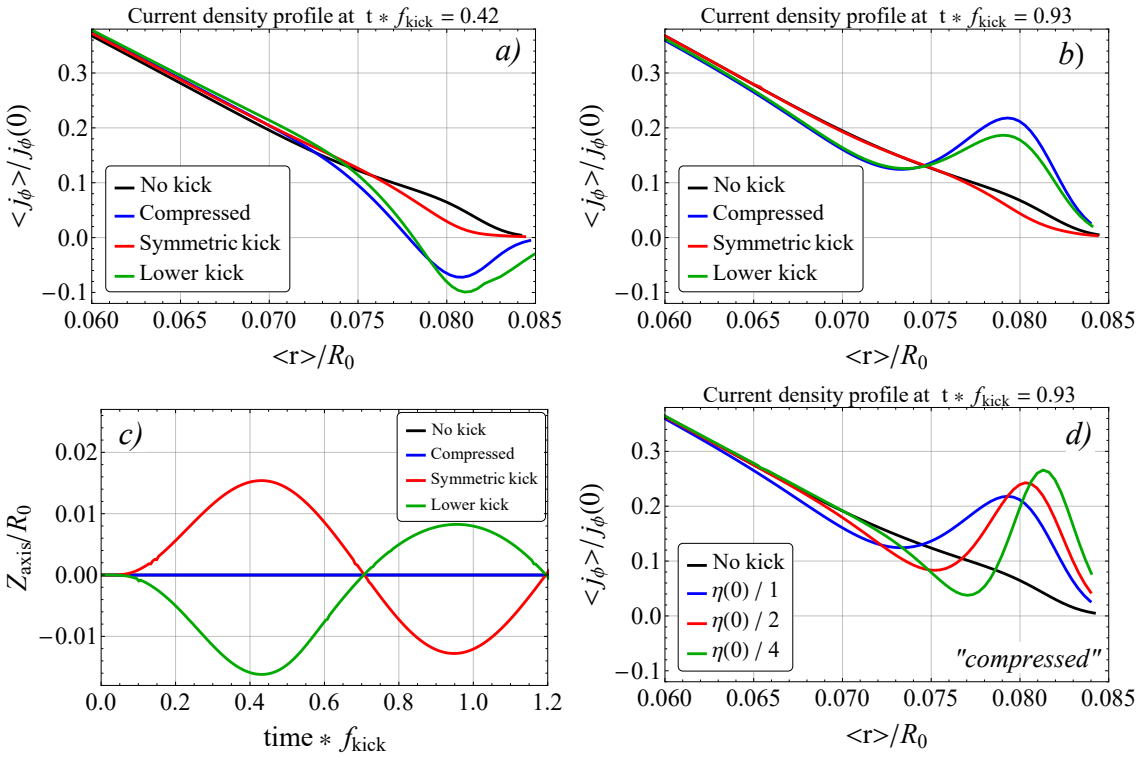

FIGURE 2: Current induction during vertical oscillations for the symmetric PF coil configuration. (a) Averaged toroidal current density in function of the averaged minor radius at time $\bar{t} = tf_{kick} = 0.42$, (b) same for time $\bar{t} = tf_{kick} = 0.93$. (c) Vertical position of the magnetic axis in function of time. (d) Averaged toroidal current in function of minor radius at time $\bar{t} = tf_{kick} = 0.93$ for different plasma resistivities (η). The legends are explained in section 2.1.1.

2.1.1 Symmetric PF coils

The first PF coil configuration respects vertical symmetry with respect to the plasma magnetic axis (Figure 1 b) and the coils (PF1/PF2) have currents with equal sign and magnitude. The VS coil currents are sinusoidally varied over time with a frequency f for 3 different current waveforms

1. **"Compressed"**: The coil currents try to compress or expand the plasma as they share equal magnitude and sign. $I_{VS1} = I_{VS2} = I_0 \sin(2\pi f t)$. No vertical motion is expected.

2. **"Symmetric kick"**: Currents have equal magnitude but different signs. $I_{VS1} = -I_{VS2} = I_0 \sin(2\pi f t)$. Vertical motion is expected.

[2] In what follows we'll use the name Vertical Stabilization (VS) coils for the coils in which currents vary over time.

3. **"Lower coil kick"**: Only the lower coil is used. $I_{VS1} = 0$ and $I_{VS2} = 2 * I_0 \sin(2\pi f t)$. Vertical motion is expected with enhanced lower displacement.

In figure 2, we show the position of the plasma center over time together with the averaged[3] toroidal current profiles at the times when the plasma reaches its extreme positions. From this figure we observe that the impact of a symmetric oscillation on the edge current is not significant. However, only using the lower coil or using both coils with the same current sign induces a significant amount of edge current. This is in agreement with our previous analytical model (equation 6) when considering the term $\delta\psi_{ext}(a_0)$ which can drive current without plasma motion. Only the cases that produce net external flux $\delta\psi_{ext}$ induce currents, the "symmetric kick" case is the only one that doesn't produce net external flux because the fluxes produced by the VS coils with different sign and same magnitude cancel. A scan on the resistivity (η) is also performed for the "compressed" case, which reveals that the penetration depth of the current increases with resistivity, it agrees quantitatively with the scaling of the skin depth $\delta_{skin} \propto \sqrt{\eta}$. As shown in figure 2 (d), increasing the resistivity by a factor 4 implies an increase of the penetration depth by a factor 2.

2.1.2 Asymmetric PF coils

The second configuration has a vertical asymmetry on the PF coils with respect to the magnetic axis (see Figure 1 b), which creates a lower X-point close to the plasma.

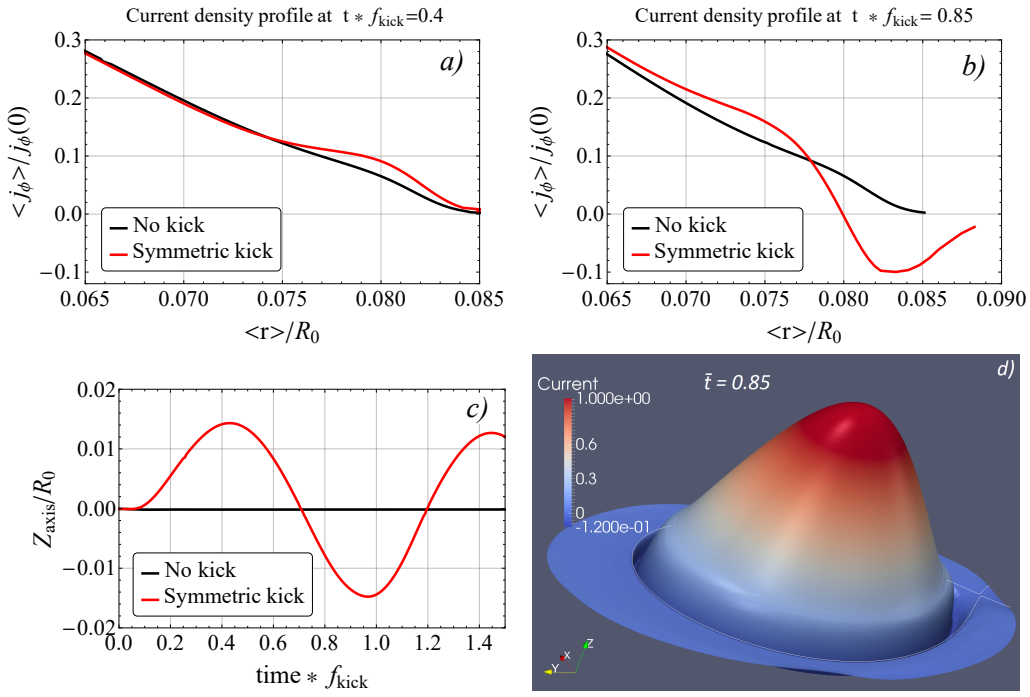

FIGURE 3: Current induction during oscillations for the asymmetric PF coil configuration. (a) Averaged toroidal current density in function of the averaged minor radius for time $\bar{t} = tf_{kick} = 0.4$ at maximal vertical position, (b) same for time $\bar{t} = tf_{kick} = 0.85$ at minimum position. (c) Vertical position of the magnetic axis in function of time. (d) Warp plot of the 2D current showing that the negative induced current is equally distributed along the flux surfaces at $\bar{t} = tf_{kick} = 0.85$.

In figure 3 we show the induced current for the case of an oscillation with symmetry in the VS coils ("symmetric kick"). When moving upwards, a small positive current is induced, but when moving towards the near X-point a significant negative current is induced. Our analytical model can explain these results by considering the terms $\delta\mathbf{r} \cdot \boldsymbol{\nabla}\psi_{ext}$ and $-B_\theta(r_0)R_0\delta w_r$ of equation (6). The magnetic field gradient is larger in the lower position and therefore when the plasma approaches PF2 it experiences a net increase of external poloidal flux which drives a current by the term $\delta\mathbf{r} \cdot \boldsymbol{\nabla}\psi_{PF2}$.

[3]Quantities with <> are averaged on the flux surfaces contours. $< A >\equiv \left(\oint_{\psi=cte} A dl\right) / \left(\oint_{\psi=cte} dl\right)$

The plasma also experiences an expansion as its lower part is more attracted by PF2 than the upper part. This enhances as well an additional decrease of current through the term $-B_\theta(r_0)R_0\delta w_r$. A more intuitive explanation for the negative sign is the fact that the plasma approaches a current with the same sign, and therefore a screening current with opposite sign is induced inside the plasma. From this point of view, we would generally expect to induce negative currents when the plasma moves towards the closest X-point. However, positive currents are induced in that situation for JET and ITER geometries. As it will be shown in the next section, ITER plasmas experience a reduction of volume in the latter case, which is the main cause of the increase in positive current.

2.2 ITER case

Here we perform an analysis of a realistic vertical oscillation with a 7.5MA/2.65T ITER H-mode scenario. This case was presented in [6] for vertical oscillation studies with the code DINA and we have used it to benchmark JOREK-STARWALL. For the benchmark we have included the same 2D axisymmetric model for the ITER wall and passive structures, which STARWALL discretises in thin triangles (see Figure 4). The vacuum vessel is modelled as two thin stainless steel layers with a width of 6 cm each, the conducting OTS (Outer Triangular Support) and DIR (Divertor Inboard Rail) are included as well.

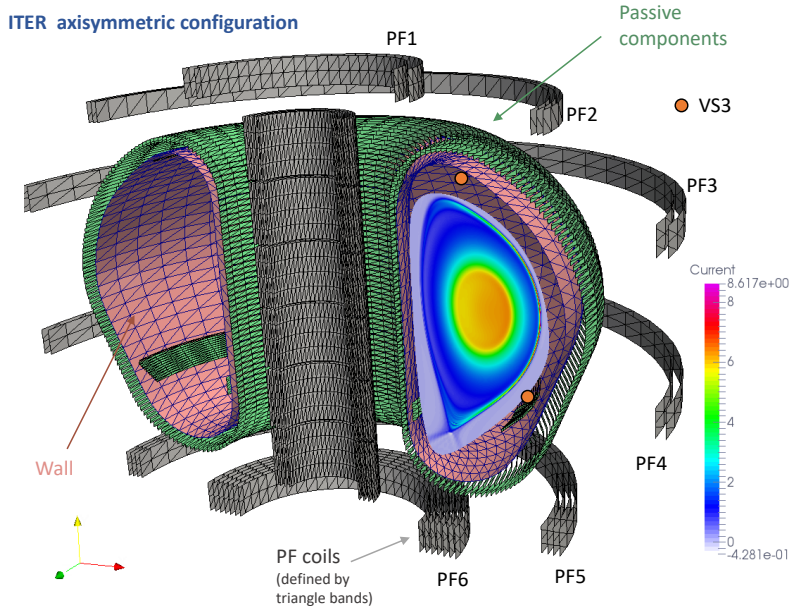

FIGURE 4: Geometrical modelling of PF coils, walls and passive structures in JOREK-STARWALL for the ITER case presented in [6].

We show the agreement of the plasma vertical position over time between JOREK-STARWALL and DINA in Figure 5. It's noteworthy that in order to get a reasonable agreement between the two codes we had to implement all the mutual inductances of the system, in particular the mutual inductance between passive components and coils was required, otherwise the plasma final displacement was overestimated by a factor 2 in some cases. This can be explained by noticing that the coils used to produce the vertical oscillation (VS3 in Figure 4) are very close to conducting components which are able to screen significantly the action of the coils.

The vertical oscillation frequency for the benchmark case was $f = 10$ Hz and the total current variation in the in-vessel coils (VS3 system) was $\Delta I_{VS3} = 240$ kA·turn. In the following simulations, we have added two extra PF coils (AUX-1, AUX-2) in order to study the influence of different coil configurations on the induction of edge current during the vertical oscillation (see figures 6 and 7). The MHD model used for these simulations [12] includes parallel flows, Bohm boundary conditions and free outflow of density and temperature at the divertor plates. As well, electric currents are set to 0 at the divertor region. The plasma grid is aligned with the initial flux surfaces and the

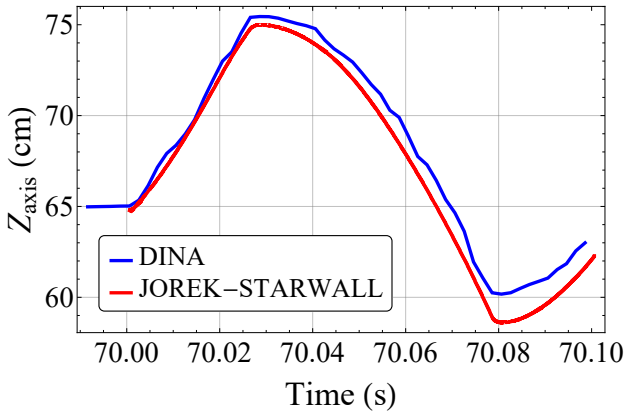

FIGURE 5: Benchmark of JOREK-STARWALL with the DINA case. The vertical position of the magnetic axis is shown over time during the vertical oscillation.

number of used Bezier elements is 24464, mesh accumulation is used as well at the pedestal and at the X-point. The pedestal gradients are maintained due to a local reduction of the density and temperature diffusivities ($D_{\perp ped} = 0.2 D_{\perp core} = 4m^2/s$, $\chi_{\perp ped} = 0.1\chi_{\perp core} = 2m^2/s$). The parallel heat diffusivity and kinematic viscosity at the core are respectively $\chi_{\parallel core} = 8.4 \times 10^9 m^2/s$ and $\nu_{\parallel core} = 20\nu_{\perp core} = 7.6 \times 10^{-6} m^2 s^{-1}$. Where the latter quantities have the following temperature dependences $\chi_{\parallel} \propto T^{5/2}$ and $\nu_{\parallel} \propto T^{-3/2}$.

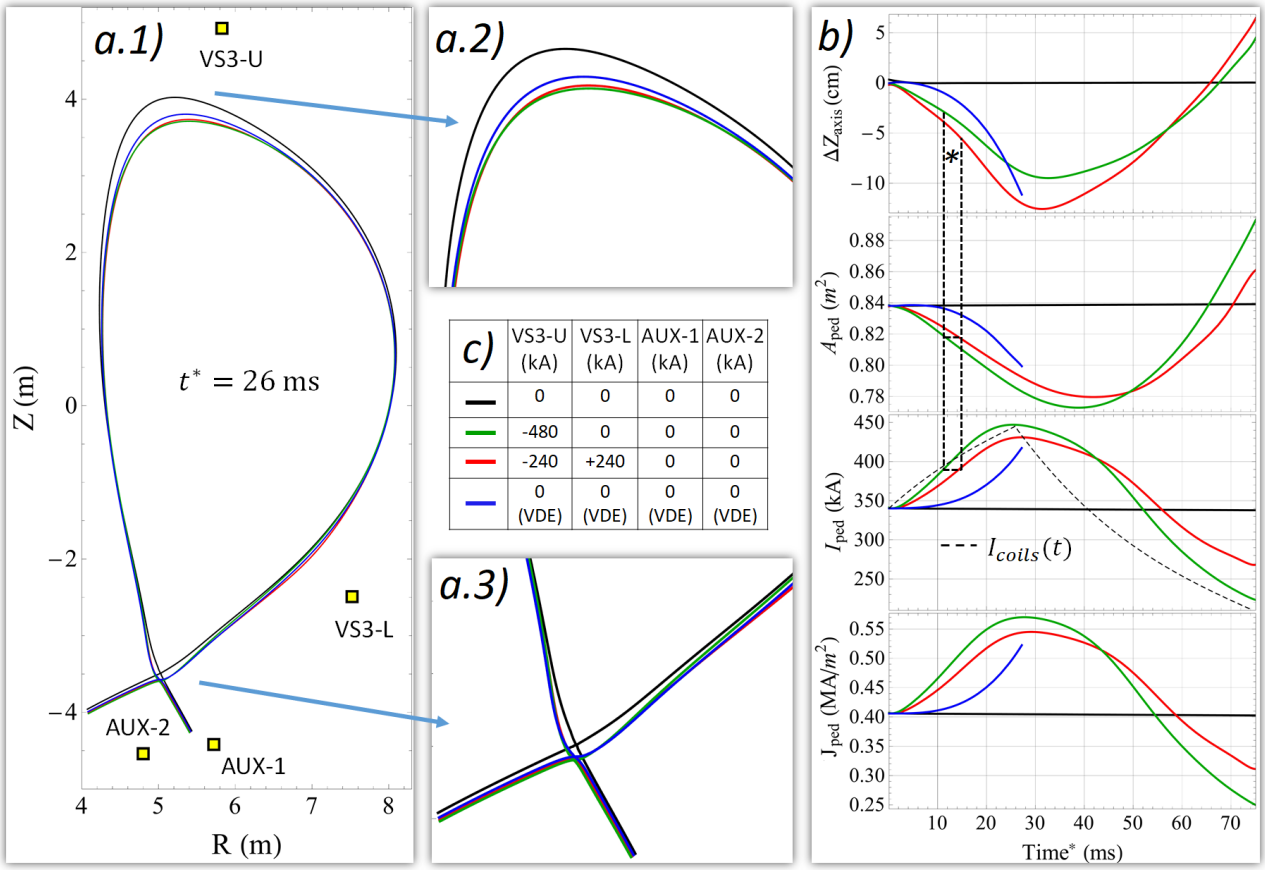

FIGURE 6: ITER current induction study for different coil configurations. a) Separatrix at $t^* = 26$ ms for different coil currents and geometries. b) Time traces of the vertical displacement of the magnetic axis ΔZ_{axis}, the pedestal area A_{ped}, the pedestal toroidal current I_{ped} and the averaged toroidal current density $J_{ped} \equiv I_{ped}/A_{ped}$. c) Maximum current used (in kA·turn) in the time-varying coils for the different cases.

Because of numerical stability related with the ELM simulations, we have increased the plasma and wall resistivities by a factor 15 as well as the oscillation frequency ($f_{new} = 150$ Hz) keeping constant the ratio τ_{kick}/τ_{η}. Finally the pedestal top resistivity corresponds to the Spitzer value for a temperature of $T_{ped,top} = 430$ eV and the separatrix to $T_{ped,sep} = 42$ eV.

We have split the study into the figures 6 and 7, where we show the different PF coil geometries, the used PF coil currents and the obtained time traces of different plasma quantities. The separatrix at time $t^* = 26$ ms[4] is also compared for the different configurations. The legend tables indicate the maximum total current used in the VS3 and AUX coils for the different cases. Note that there is a special time trace (dark blue), where we have increased the wall resistivity by a factor 10 such that a natural VDE was destabilised. For that case, the chosen wall resistivity was such that the the plasma moved downwards with a similar time scale and displacement as the oscillation cases, this case allows us to study the current induction without the influence of time-varying coil currents.

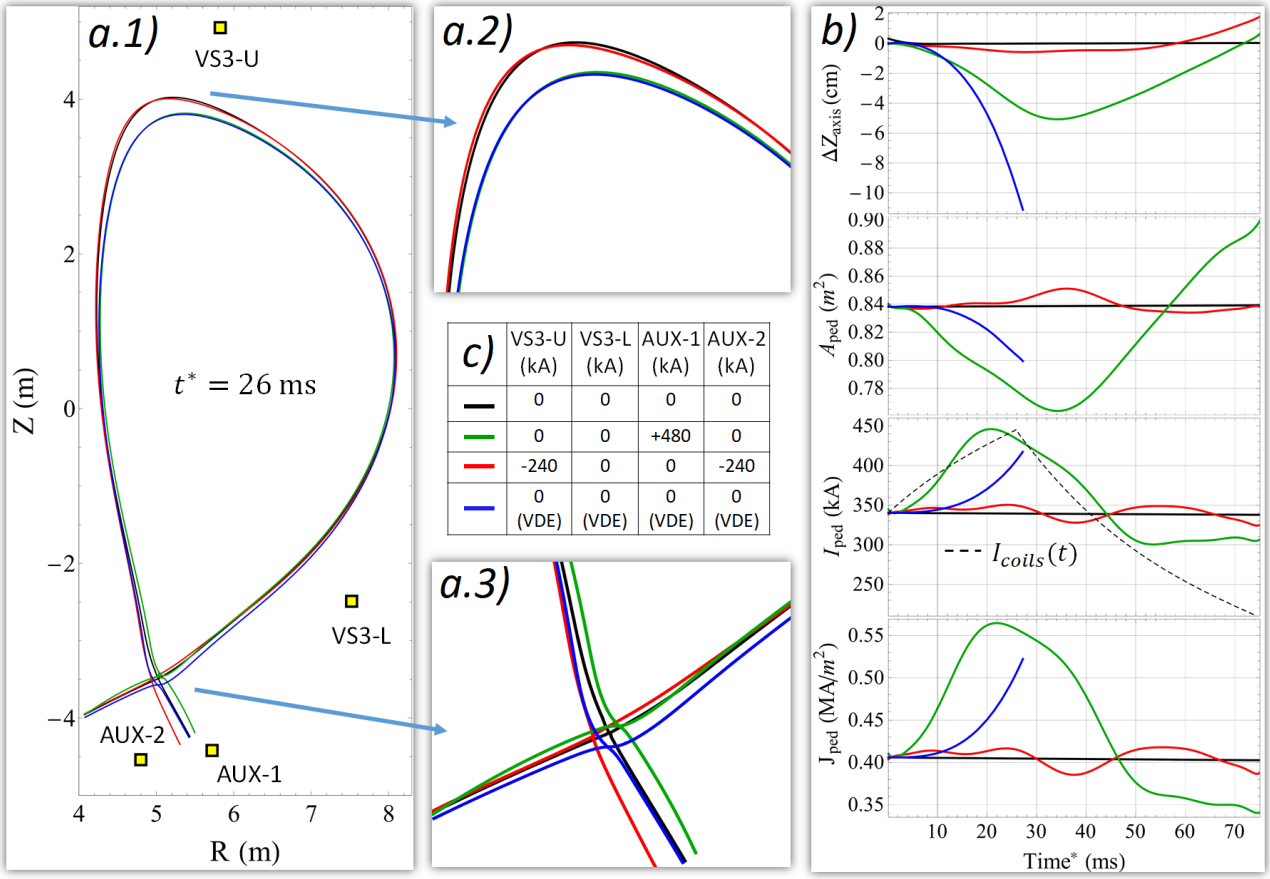

FIGURE 7: ITER current induction study for different coil configurations. a) Separatrix at $t^* = 26$ ms for different coil currents and geometries. b) Time traces of the vertical displacement of the magnetic axis ΔZ_{axis}, the pedestal area A_{ped}, the pedestal toroidal current I_{ped} and the averaged toroidal current density $J_{ped} \equiv I_{ped}/A_{ped}$. c) Maximum current used (in kA·turn) in the time-varying coils for the different cases.

The cases where more current I_{ped} is induced are the cases in which the plasma develops a larger reduction of the pedestal cross-sectional area A_{ped} (see Figures 6 b and 7 b). It should be noted that some coil configurations are more efficient than others reducing the plasma cross-section and thus inducing current. For example to use only the upper VS3 coil (green curve in figure 6) is more efficient than to use the ITER baseline oscillation where both VS3 coils are used (red curve in figure 6). In order to obtain the same $I_{ped} = 390$ kA, the baseline configuration requires a vertical displacement of $\Delta Z_{axis} = 5.5$ cm while only using the upper VS3 coil requires $\Delta Z_{axis} = 3$ cm (see figure 6 b*). The compression can be also enhanced by moving the position of the X-point with the AUX coils (see green curve in figure 7).

[4]for clarity, we define the re-scaled time as $t^* \equiv 15 \times t_{simulated}$

The VDE case is very similar to the baseline case in terms of current induction, comparable currents are induced at similar positions and pedestal areas (see figure 6 b). From this observation it can be concluded that the time-varying coil currents do not directly influence the pedestal current, but it's rather the subsequent plasma motion that causes the compression and induces current. Therefore the term $\delta\psi_{ext,coils}(a_0)$ of equation (6) has little impact in this case. If that term was the dominant one, the case where the plasma position has been kept fixed and the coil currents aim to compress the plasma would have induced a significant current (see red curve of Figure 7).

The change in plasma cross section is due to the fact that the top of the plasma (see figure 6 a.2) moves faster than the X-point (see figure 6 a.3). This effect is due to the vertical asymmetry of the external magnetic field produced by the PF coils. Therefore we expect a weaker induction of current for double-null plasmas. In Figure 8 we show the change in external flux along the poloidal angle θ of the flux surface $\psi_N = 0.98$[5], the flux difference is taken after a downward displacement of $\Delta Z_{axis} = -1.4$ cm. The change in total external flux (blue curve) is separated into the contributions due to the currents in the walls and passive structures, the currents in the VS3 coils and the motion through the static field produced by the PF coils (motional effect). The figure reveals that total change in external flux ($\delta\psi_{ext}$) is determined by the motional effect contribution ($\delta\mathbf{r}\cdot\boldsymbol{\nabla}\psi_{PF}$) while the other contributions cancel approximately each other.

As an overall conclusion, the increase in pedestal current arises from the motion of the plasma through the asymmetric magnetic field produced by the PF coils. During the vertical motion, the reduction of plasma cross-section and the variation of external flux cause an increase of current through the terms $-B_\theta(r_0)R_0\delta w_r$ and $\delta\mathbf{r}\cdot\boldsymbol{\nabla}\psi_{PF}$ of equation 6. As well, plasma compression can be enhanced by using different coil configurations to move the plasma.

Finally the time traces also show that the change in the averaged current density δJ_{ped} is dominated by the change in total current $\delta I_{ped}/I_{ped} \sim 23\%$ rather than the change in the pedestal area $\delta A_{ped}/A_{ped} \sim 8\%$.

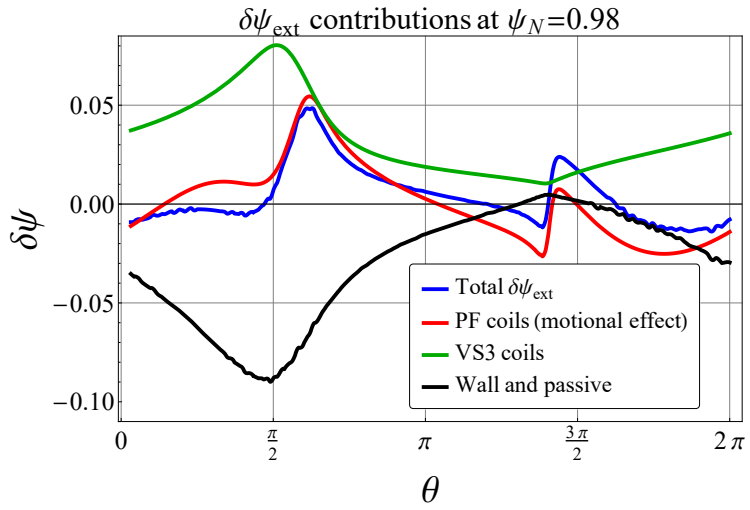

FIGURE 8: External flux variation at the $\psi_N = 0.98$ flux surface after a downward displacement of -1.4 cm. θ is the angle along the flux poloidal contour and the curves represent the different contributions to $\delta\psi_{ext}$. This case corresponds to the oscillation with $I_{VS3L} = -I_{VS3U} = 240$ kA. The flux difference is done with a small ΔZ in order to keep the plasma deformation small so the angle θ still identifies correctly the displaced position.

[5]The radial coordinate ψ_N is the normalized poloidal flux, being 1 at the separatrix and 0 at the plasma core.

3 ELM triggering for an ITER plasma

In this section we study the stability of the latter ITER case. As a reminder, the frequency of the vertical motion was scaled by a factor 15 ($f = 10 \rightarrow 150$ Hz) as well as the wall and plasma resistivities in order to keep the ratio τ_{kick}/τ_η constant. Unless noted otherwise, the vertical oscillation is performed with the ITER baseline coil configuration (VS3 U/L) with maximum current amplitudes of 240 kA·turn per coil. As our main interest is to show the ELM destabilization principle, we only consider the toroidal mode number $n = 6$ interacting non-linearly with the axisymmetric mode $n = 0$ for the sake of simplicity. More realistic simulations would require to include diamagnetic and neoclassical flows in our model in order to stabilize high-n mode numbers, we leave this task for future work.

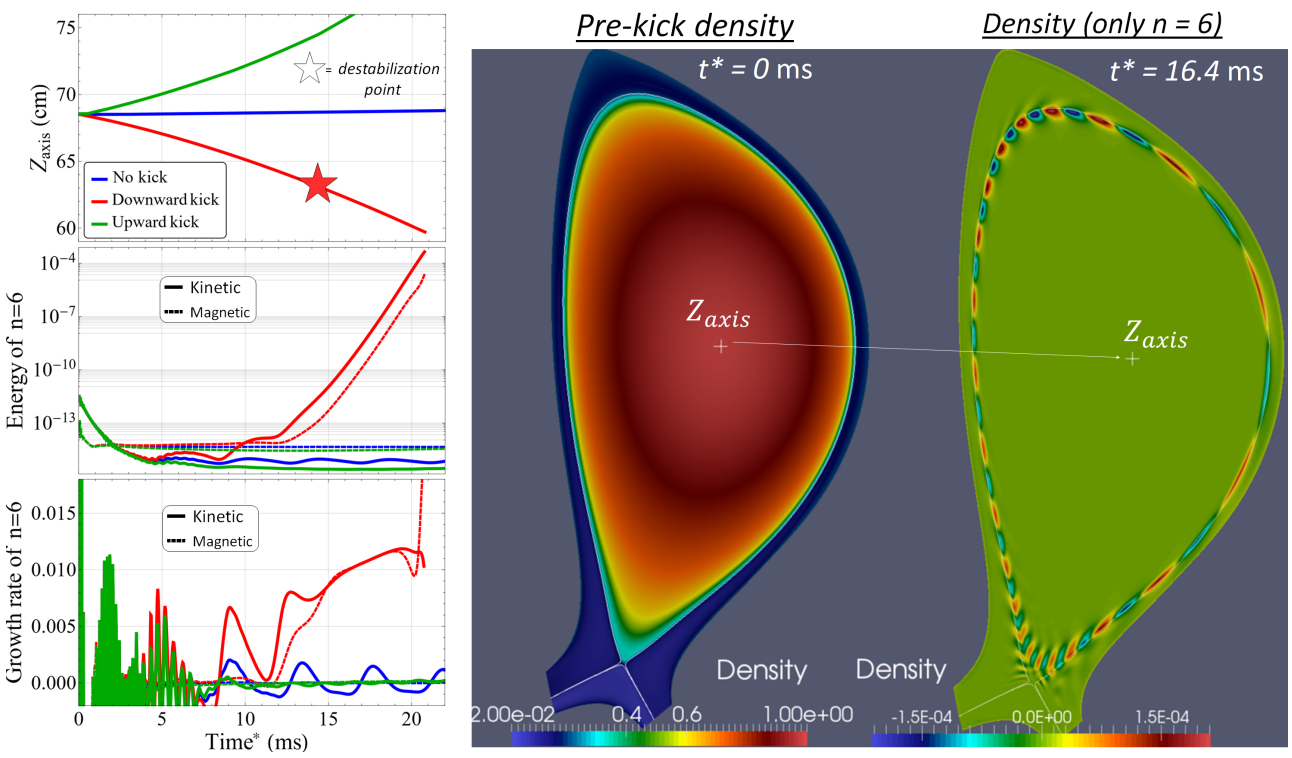

FIGURE 9: (Left) Time traces of the position of the magnetic axis, the normalized energies and growth rates of the mode $n = 6$. (Right) Pre-kick plasma density and the destabilized $n = 6$ linear mode structure of the density.

In Figure 9 we present an example of how an initially stable $n = 6$ mode can be destabilized by applying a vertical downward motion. The destabilized mode structure presents the characteristics of a peeling-ballooning mode [7] formed close to the plasma separatrix. We define the destabilization point as the time in which the magnetic and kinetic growth rates agree within 10 % and a mode structure is clearly formed. An upward vertical motion was also applied and does not lead to the triggering of an ELM. In order to study in more detail the effect of the upward motion, we repeat the same study for an initially unstable case and we analyse its influence on the growth rate.

The study shown in Figure 10 reveals that a downward motion can further destabilize an initially unstable peeling-ballooning mode by increasing its growth rate. As well, the upward motion case is able to decrease the growth rate down to negative values and stabilize the mode. A comparison of the current and pressure gradient profiles at points with increasing, constant and decreasing growth rate show that the destabilizing mechanism can be related with the current profile. The total current inside the pedestal and the current gradient at the separatrix may be good candidates for destabilizing mechanisms. It's worth noting that the pressure gradient increases during the downward motion and therefore it could also be a destabilizing factor.

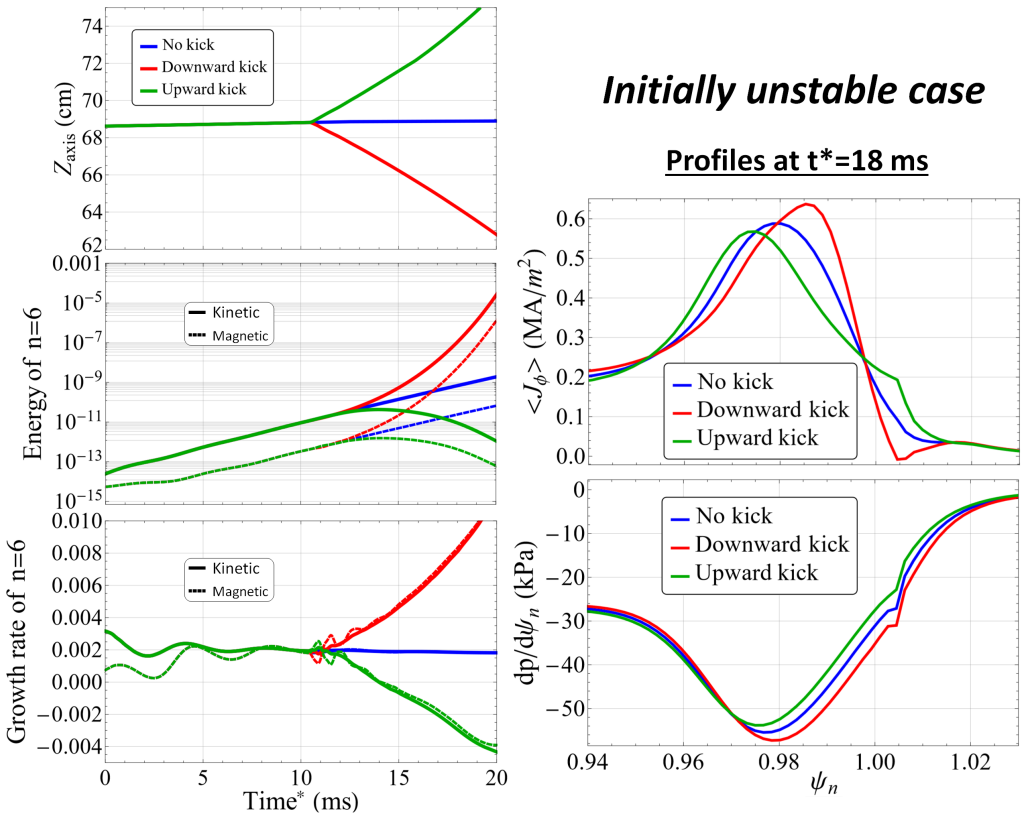

FIGURE 10: (Left) Time traces of the position of the magnetic axis, the normalized energies and growth rates of the mode $n = 6$. (Right) Averaged toroidal current and pressure gradient profiles at $t^* = 18$ ms. For this particular case, the time-scale of the motion τ_{kick} has been reduced by a factor 2 to better observe the change in the growth rates before reaching the non-linear phase of the downward kick case.

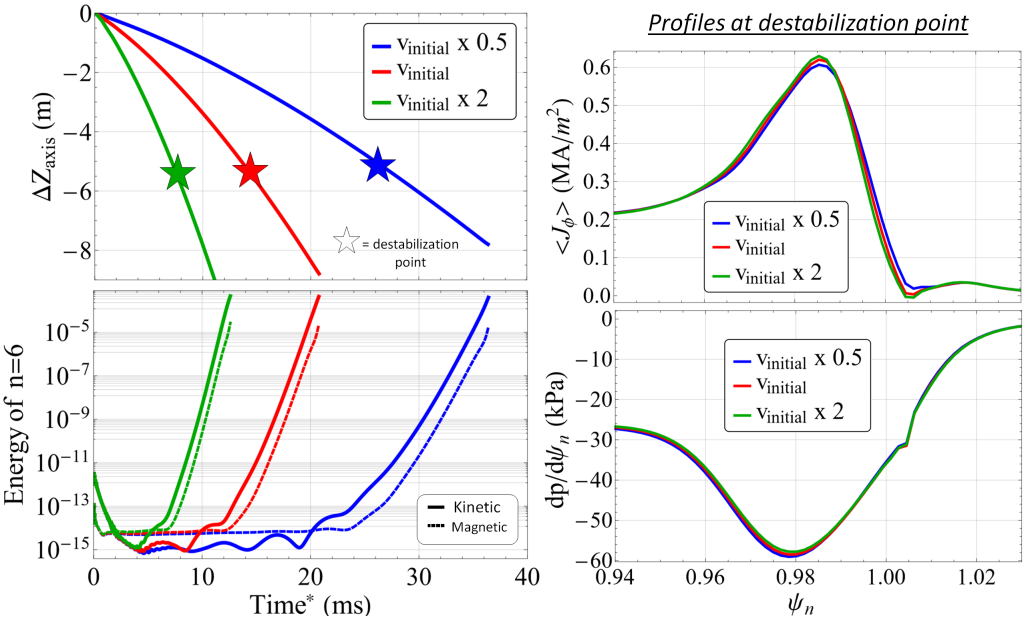

FIGURE 11: (Left) Time traces of the position of the magnetic axis and the normalized energies of the mode $n = 6$. (Right) Averaged toroidal current and pressure gradient profiles at the destabilization point.

Experiments in JET [3] demonstrated that the ELM triggering strongly depends on the plasma displacement ΔZ_{axis} but not on the plasma velocity during the oscillation. In Figure 11 we perform a scan on the plasma vertical velocity for a downward motion. For an initially stable case, an ELM was destabilized at the same vertical displacement ($\Delta Z_{axis} \approx 5.5$ cm) for the three cases with different vertical velocities in agreement with experimental observations. If we assume that the induced edge

current is the main cause of the ELM destabilization, this could be well explained by the prediction of equation 6, where the plasma speed only plays a role through the resistive decay term (which is expected to be very small for hot plasmas). At the destabilization point, the current and pressure gradient profiles were very similar, supporting the idea that the ELM triggering can be described in terms of the stability of equilibrium states, i.e. it does not depend on the kick velocity.

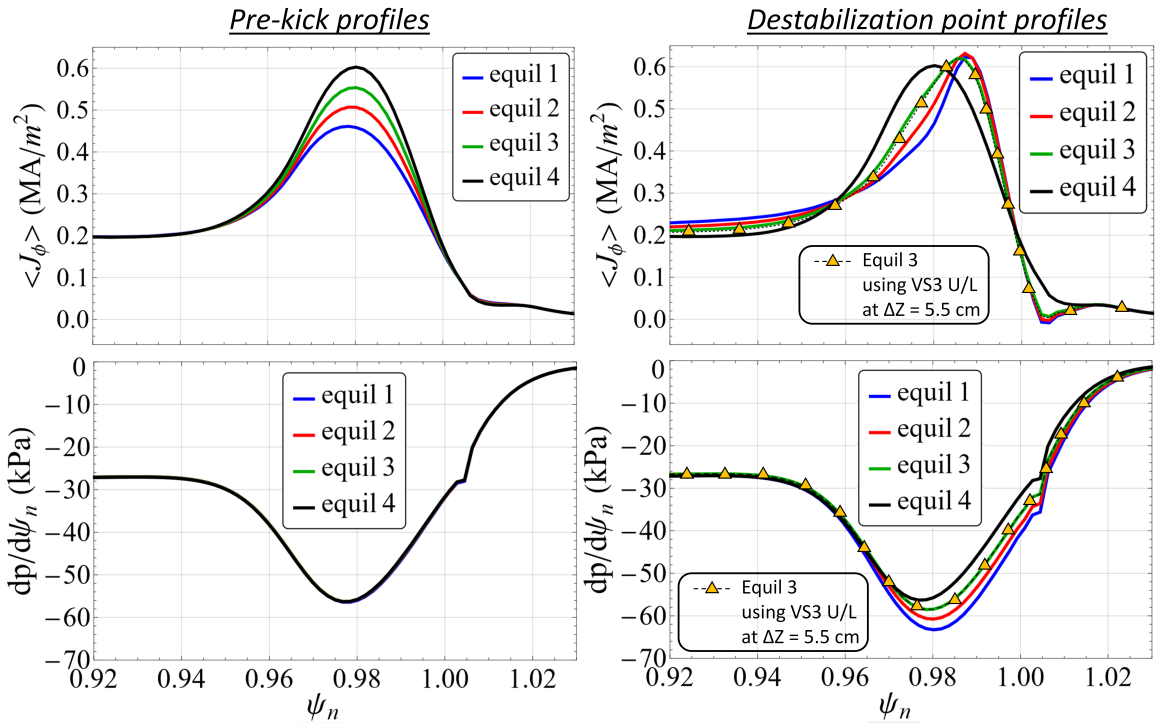

FIGURE 12: Profiles for the vertical oscillation shown in (Figure 13). (Left) Initial current and pressure profiles. (Right) Profiles at the destabilization points. For reference, the dashed curve indicates the profiles at the destabilization point when using the baseline coil configuration (see Figure 9), where the starting equilibrium corresponds to the green curve.

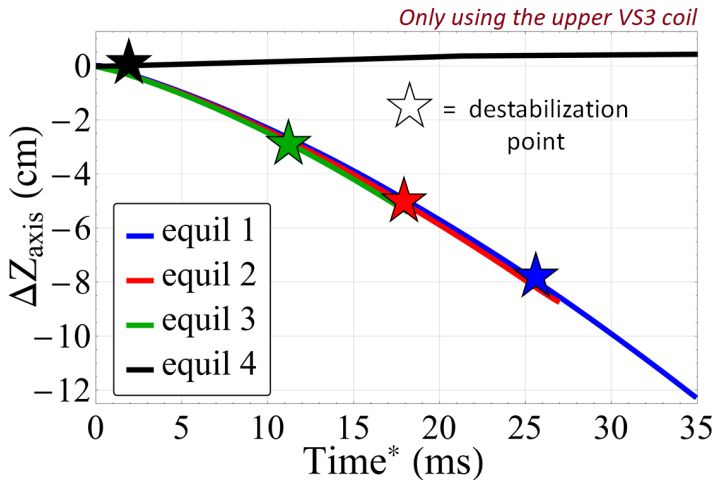

FIGURE 13: Plasma vertical displacement with time for the different starting equilibria (Figure 12). The destabilization points are marked with a star symbol.

In order to further explore the relation of the induced edge current and the ELM triggering, we perform the same vertical motion on four different starting equilibria. For this vertical oscillation only the upper VS3 coil has been used as this coil configuration induces more current for smaller

displacements[6]. The different starting equilibria have the same pressure profile but different averaged current profiles (Figure 12 "pre-kick profiles"). If the instability is triggered by an increase of edge current during the vertical motion, we expect to require bigger ΔZ_{axis} for lower initial edge currents. Indeed, the results shown in Figure 13 support this hypothesis. Moreover, the destabilization occurs when the current density values become comparable to the initially unstable case, i.e. the black curve. As it can be observed, the pressure profiles also vary during the motion, this is due to the adiabatic compression of the pedestal that follows the law $PV^{\gamma} = cte$. Therefore the evolution of the pressure profile may also be relevant to trigger the instability. However, the starting pressure profiles were identical in all the cases and they present different peak values at the destabilization points which shows that the main destabilizing factor is the edge current. In addition the mode structure has a strong peeling component (Figure 9) which reinforces the idea of the current as the main destabilizing mechanism.

4 Conclusions

ELM triggering via vertical oscillations has been performed in the TCV[1], AUG [2] and JET [3] tokamaks proving to be a reliable technique for the ELM frequency control. In this paper, the physics of the ELM triggering mechanism via vertical oscillations was studied for the first time in non-linear MHD simulations with the free-boundary code JOREK-STARWALL.

References [3, 6] propose the induction of edge current during the vertical oscillation to be the destabilizing mechanism for an ELM. In this paper, a simple analytical model was derived in order to illustrate the origin of this current (equation 6), showing it to be independent on the speed of the vertical motion for ideal plasmas and to result from a change on the boundary external flux and plasma compression. The edge current induction was also studied with JOREK-STARWALL for a simple elongated plasma and for a realistic ITER scenario. For the simple case, the analysis showed that the induced current can be understood as a screening current reaction of the plasma against the change of external magnetic flux, either if the change is produced by a strong asymmetry in the VS coils ($\delta\psi_{VS}(a_0)$) or by the plasma motion through an inhomogeneous magnetic field ($\delta\mathbf{r}\cdot\boldsymbol{\nabla}\psi_{PF}$). The ITER case revealed that the induced edge current can also be strongly related to the plasma compression due to its motion through the top-down asymmetric magnetic field. In addition, figures 6 and 7 indicate that the compression and the induced current can be enhanced by choosing different geometries and current waveforms for the coils used to displace the plasma.

The phenomenon of ELM destabilization via vertical oscillations was simulated in a consistent dynamic scheme for the first time. An initially stable $n = 6$ mode was found to be destabilized by a downward motion and to remain stable when applying an upward one (see Figure 9). The destabilized mode has the structure of a peeling-ballooning mode. Additional simulations with an initially unstable plasma (figure 10) revealed that the mode was stabilized by the upward motion and further destabilized by a downward one. Figure 13 revealed that the pre-kick edge current profile is strongly related with the minimum plasma displacement required to destabilize the mode, requiring bigger displacements for lower initial edge currents. In agreement with experiments, the destabilization does not depend on the plasma velocity but on the plasma displacement ΔZ_{axis} (figure 11). For practical applications, the minimum vertical displacement that is required for ELM triggering will strongly depend on the bootstrap current. In our baseline scenario ELMs were destabilized for displacements of 5-6 cm, these displacements could be performed at ITER without exceeding the VS3 system limits for typical oscillation frequencies of $10 - 15$ Hz and maximum currents of $I_{VS3} = 160 - 200$ kA·turn [6].

The simulations confirm the hypothesis of the induced edge current as the essential mechanism for the ELM destabilization. The requirement of larger displacements for lower initial currents and the fact that the edge current increases for downward motions reinforce the idea of the edge current as the main destabilizing factor. As well, the destabilized mode presents a strong peeling structure. This mechanism can also explain the weak dependence of the ELM triggering on the vertical speed

[6]this choice was made in order to avoid large displacements that can lead the plasma to touch the boundary of our flux-aligned grid.

as indicated by equation (6). The role of pressure profile modifications during the kick may not be negligible as well and will require further investigations.

Disclaimer

The views and opinions expressed herein do not necessarily reflect those of the ITER Organization.

Acknowledgements

The authors acknowledge access to the EUROfusion High Performance Computer (Marconi-Fusion) through EUROfusion funding.

References

[1] AW Degeling et al. "Magnetic triggering of ELMs in TCV". In: *Plasma physics and controlled fusion* 45.9 (2003), p. 1637. DOI: 10.1088/0741-3335/45/9/306.

[2] PT Lang et al. "Frequency control of type-I ELMs by magnetic triggering in ASDEX Upgrade". In: *Plasma physics and controlled fusion* 46.11 (2004), p. L31. DOI: 10.1088/0741-3335/46/11/102.

[3] Elena de la Luna et al. "Understanding the physics of ELM pacing via vertical kicks in JET in view of ITER". In: *Nuclear Fusion* 56.2 (2015), p. 026001. DOI: 10.1088/0029-5515/56/2/026001.

[4] M Hölzl et al. "Coupling JOREK and STARWALL codes for non-linear resistive-wall simulations". In: *Journal of Physics: Conference Series*. Vol. 401. 1. IOP Publishing. 2012, p. 012010. DOI: 10.1088/1742-6596/401/1/012010.

[5] A Loarte et al. "Progress on the application of ELM control schemes to ITER scenarios from the non-active phase to DT operation". In: *Nuclear Fusion* 54.3 (2014), p. 033007. DOI: 10.1088/0029-5515/54/3/033007.

[6] Y Gribov et al. "Plasma vertical stabilisation in ITER". In: *Nuclear Fusion* 55.7 (2015), p. 073021. DOI: 10.1088/0029-5515/55/7/073021.

[7] GTA Huysmans. "ELMs: MHD instabilities at the transport barrier". In: *Plasma Physics and Controlled Fusion* 47.12B (2005), B165. DOI: 10.1088/0741-3335/47/12b/s13.

[8] SH Kim et al. "Comparing magnetic triggering of ELMs in TCV and ASDEX Upgrade". In: *Plasma Physics and Controlled Fusion* 51.5 (2009), p. 055021. DOI: 10.1088/0741-3335/51/5/055021.

[9] GTA Huysmans and O Czarny. "MHD stability in X-point geometry: simulation of ELMs". In: *Nuclear fusion* 47.7 (2007), p. 659. DOI: 10.1088/0029-5515/47/7/016.

[10] P Merkel and E Strumberger. "Linear MHD stability studies with the STARWALL code". In: *arXiv preprint arXiv:1508.04911* (2015). URL: https://arxiv.org/abs/1508.04911.

[11] S Jardin. *Computational methods in plasma physics*. CRC Press, 2010. DOI: 10.1201/ebk1439810958.

[12] GTA Huysmans et al. "Non-linear MHD simulations of edge localized modes (ELMs)". In: *Plasma Physics and Controlled Fusion* 51.12 (2009), p. 124012. DOI: 10.1088/0741-3335/51/12/124012.